JOURNAL OF SOLID STATE CHEMISTRY 118, 141–147 (1995)

Structures in the Oxygen-Deficient Fluorite-Related R_nO_{2n-2} Homologous Series: $Pr_{10}O_{18}$

J. Zhang, R. B. Von Dreele,* and L. Eyring

*Department of Chemistry and Biochemistry and the Center for Solid State Science, Arizona State University, Tempe, Arizona 85287-1604; and *Manuel Lujan, Jr. Neutron Scattering Center, LANSCE, MS H805, Los Alamos National Laboratory, Los Alamos, New Mexico 87545*

Received April 8, 1994; in revised form March 3, 1995; accepted March 7, 1995

The crystal structure of $Pr_{10}O_{18}$ was determined utilizing Rietveld analysis of neutron time-of-flight (TOF) powder diffraction data. Despite the large size of the unit cell and the complexity of the structure, the refinement was successful ($P2_1/c$, a = 6.7304(5) Å, b = 19.390(1) Å, c = 12.794(1) Å, β = 100.213(1)°, V = 1643.2(4) Å^3, and Z = 4; 150 total variables, R_p = 2.93%, wR_p = 4.30%). The basic structural element is a pair of vacant oxygen sites separated by a $\frac{1}{2}\langle 1\ 1\ 1\rangle_F$ vector across a metal atom, similar to those observed in the more reduced members of the Pr_nO_{2n-2} series, Pr_7O_{12} and Pr_9O_{16}. However, the arrangement of the vacancy pairs is different than the models previously proposed on the basis of high-resolution electron microscopy. © 1995 Academic Press, Inc.

INTRODUCTION

Early thermodynamic studies on the PrO_x–O_2 system indicated that $Pr_{10}O_{18}$ (ε) was one of the stable oxygen-deficient fluorite-related intermediate oxides in the Pr_nO_{2n-2} homologous series (1–4). The splitting patterns of the substructure reflections were examined in these experiments, and pseudo-cell dimensions were derived. The relationship of ε with the parent fluorite structure was established by means of electron diffraction (5). Based on the relationship of its transformation matrix to that of fluorite, $Pr_{10}O_{18}$ was classified as a member of the monoclinic (n-even) branch of the homologous series. The electron diffraction study also indicated that the unit cell content was $Pr_{40}O_{72}$. Such a large unit cell presents a formidable challenge for structure determination.

Previous efforts utilizing single crystal X-ray diffraction to determine the ordering of the vacant oxygen sites in $Pr_{10}O_{18}$ were not successful (6), owing to the fact that the specimen might have been twinned, and the very large (μ = 400 cm^{-1}) absorption correction for the X-ray data was crucial and difficult to determine. The resolution of neutron powder diffraction instruments available at the time was limited and therefore it was not possible to acquire adequate data to solve such a complex structure by means of Rietveld analysis. Nevertheless, the single crystal X-ray studies did suggest that the space group of $Pr_{10}O_{18}$ was $P2_1/c$. By applying high-resolution electron microscopy and image simulation, which had become a promising method for obtaining structural information, a model for $Pr_{10}O_{18}$ was proposed in the space group $P2_1/c$ (7). Later, during a study of electron-beam-induced chemical reduction of $Pr_{24}O_{44}$ (β_1), a different structure model with $P\bar{1}$ symmetry was derived for $Pr_{10}O_{18}$, based on the assumption that β_1 and ε, both even members of the homologous series, shared the common (0 1 0) = $(0\ 2\ 2)_F$ planes composed of oxygen vacancy pairs (8). This model was further elaborated in a paper that considered the consequences of the symmetry relationships imposed by the group-theoretical family tree (9).

During the past few years, the resolution of neutron time-of-flight powder diffraction was greatly improved at Los Alamos National Laboratories. In addition, an advanced structure determination package based on Rietveld refinement, GSAS (10), became available. These developments provided a unique opportunity to clarify the conflicting results and ambiguities in the previous investigations of the structure of $Pr_{10}O_{18}$ as well as the other members of the homologous series of higher oxides of the rare earths. As the structures of Pr_7O_{12} (11), Pr_9O_{16} (12), and Tb_7O_{12} and $Tb_{11}O_{20}$ (13) were determined for the odd-number subgroup of the homologous series, it became increasingly urgent to understand the differences between the odd and even branches at the atomic level. In addition, solving the structure of $Pr_{10}O_{18}$ would further establish the capability of the Rietveld analysis technique for determining large, complex, unknown structures.

EXPERIMENTAL

Sample preparation. The $Pr_{10}O_{18}$ sample for the powder neutron diffraction study was prepared following procedures and conditions previously established (2). The starting material Pr_6O_{11} (Research Chemicals Inc., of 5N purity) was heated at 1000°C for several hours to remove

0022-4596/95 $12.00

possible contamination from carbonates and hydroxides formed during storage. The product was light green, characteristic of the A-type Pr_2O_3. The composition was adjusted to $Pr_{10}O_{18}$ by annealing the sample under 14 Torr of O_2 at 460°C for 6 days to ensure homogeneity. The sample was sealed off at 460° under conditions such that any absorption of the gaseous oxygen during cooling would be insufficient to change significantly the composition of the relatively large sample of oxide. The sample thus prepared was kept and transferred under inert atmospheres into airtight vanadium cans for neutron diffraction studies.

Neutron diffraction and Rietveld analysis. The neutron TOF diffraction data were collected at room temperature on the high-resolution instrument (NPD) at the Manuel Lujan, Jr. Neutron Scattering Center at the Los Alamos National Laboratories. The data set comprised four time-of-flight spectra from detectors at 2θ of $\pm 148°$ and $\pm 90°$, respectively. The Rietveld refinements were performed utilizing the GSAS structure analysis package (10). Variables such as background, scale factors, diffractometer constants, and profile coefficients were adjusted while using a pseudo-fluorite unit cell as the initial structure model. The cubic symmetry of the fluorite cell was removed by introducing small distortions, and the lattice constants were refined to fit the strong substructure reflections.

MODELING AND TESTING

As has been proven, the most critical step in structure determination through Rietveld analysis is to obtain reasonable initial models. This is particularly true in the present work. Since the unit cell of $Pr_{40}O_{72}$ is large and the variables are numerous, the testing of each model through least-squares refinements is a time-consuming process. Therefore, it is mandatory to reduce the number of possible models as far as possible.

The model previously proposed in space group $P2_1/c$ (6, 7) (Fig. 1a) was tested first. The selection of this space group was based on the following considerations. Previous single crystal X-ray diffraction work suggested that both $Pr_{10}O_{18}$ and $Pr_{12}O_{22}$ were monoclinic and in space group $P2_1/c$. The occupancies of two unique oxygen sites were assigned to zero, and the rest of the input atomic positions were adjusted accordingly to reflect the distortions of the vacancy clusters from the parent fluorite structure. The lattice constants of the monoclinic cell were refined, followed by gradual release of the positional parameters. The refinement always led to unreasonably short O–O and/or O–Pr distances, regardless of the sequence of the atoms involved in the refinement. This indicated that the model was incorrect.

Other alternative models were searched for in space group $P2_1/c$. The recent structure determination of $Pr_{12}O_{22}$, utilizing neutron powder diffraction and Rietveld analysis, has proven this space group for $Pr_{12}O_{22}$ to be correct (14). The credibility of the results from the X-ray diffraction studies was thus supported. In addition, the observed superstructure reflections could be indexed with a monoclinic cell with $P2_1/c$ symmetry, even though there was an apparent disparity between the calculated and observed intensities at this point. The $P\bar{1}$ model (8) would double the number of unique atoms to 56 and require a substantial increase in computing time. Therefore, efforts to solve the structure in $P2_1/c$ were pursued.

Apart from this, there were seven other possibilities with $P2_1/c$ symmetry given (6, 7). All of them were derived based on the assumption that the unit cell origin was on a metal atom. Careful examination of these models suggested that six of them should be discarded because they either involved aggregates of more than two oxygen vacancies ($\square_O$) with short separations of $\frac{1}{2}\langle 1\ 1\ 1\rangle_F$, or overlapping of oxygen atoms from two adjacent $\square_O Pr_4O_6$ defect clusters. (See Ref. (12) for descriptions of the defect clusters.) Since such arrangements have not been observed in any other known structures of the intermediate phases more oxidized than R_7O_{12}, it was assumed that they were unstable, and therefore the associated models should not be considered further. The only remaining possibility involved vacancy pairs separated by $\frac{1}{2}\langle 1\ 1\ 1\rangle_F$ without a metal atom in between. Such fragments were known to be relatively unstable compared with the double vacancy clusters in the more reduced oxides (12) (Fig. 1b), and this might have been the reason that this model was eliminated in the previous work (6, 7). However, the assumed necessity that the unit cell origin must be on a metal atom had eliminated half of the possibilities. When the $(1\ \bar{1}\ 1)_F$ metal planes were shifted by $\frac{1}{8}c_\varepsilon$, another set of eight models were generated from those examined previously (6, 7, 15). Among these possibilities, the model in Fig. 1c transformed from Fig. 1b appeared promising; furthermore, it was the only one that did not have unfavorable vacancy arrangements.

Further refinement of this new model was successful. To avoid problems caused by the pseudo-symmetry, distortions from the fluorite structure were introduced into the initial model according to the patterns observed in Pr_9O_{16}, which is composed of similar $[\square_O Pr_3Pr_{1/2}O_6]_2$ double vacancy clusters (12). The isotropic thermal factors of like atoms were refined as one parameter in an effort to reduce the number of variables. The atom positions made minor shifts when the positional parameters were refined, and the resulting interatomic distances were reasonable. The calculated spectra are in good agreement with those observed (e.g., Fig. 2). The low values of R_p, wR_p, and reduced χ^2 also support the reliability of the refinement (Table 1).

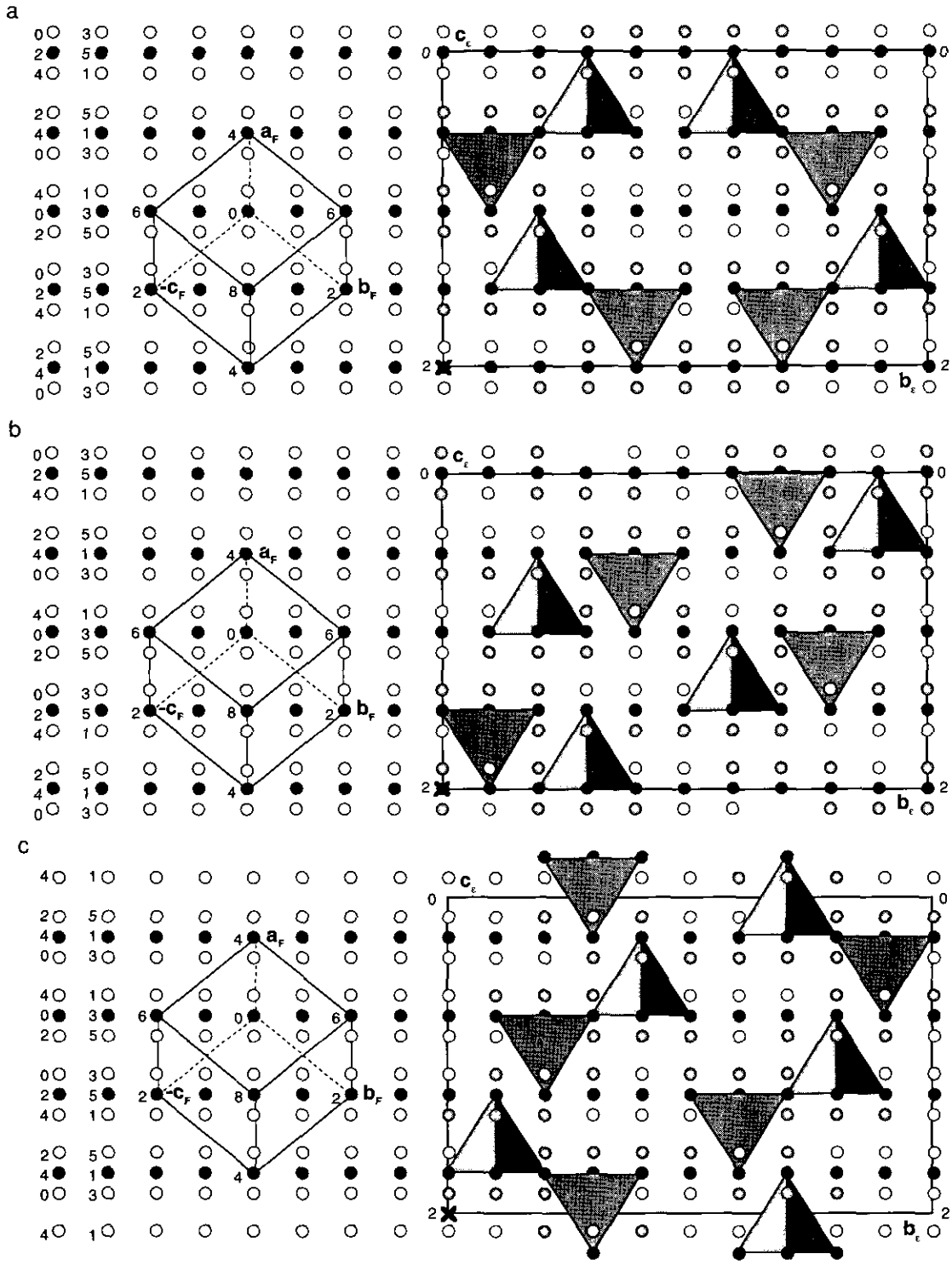

FIG. 1. The $[1\,0\,0]_\varepsilon$ projections of the structure models considered. The vacancy clusters, $\square_O Pr_4O_6$ or $(\square_O)_2Pr_7O_{12}$, are outlined. (Solid circles: Pr atoms; shaded circles: O atoms in the vacancy clusters; open circles: O atoms that are not associated with vacancy clusters.) (a) The model proposed in Ref. (7). (b) The model with $\frac{1}{2}\langle 1\,1\,1\rangle$ vacancy separation but no metal atom. (c) The correct structure model.

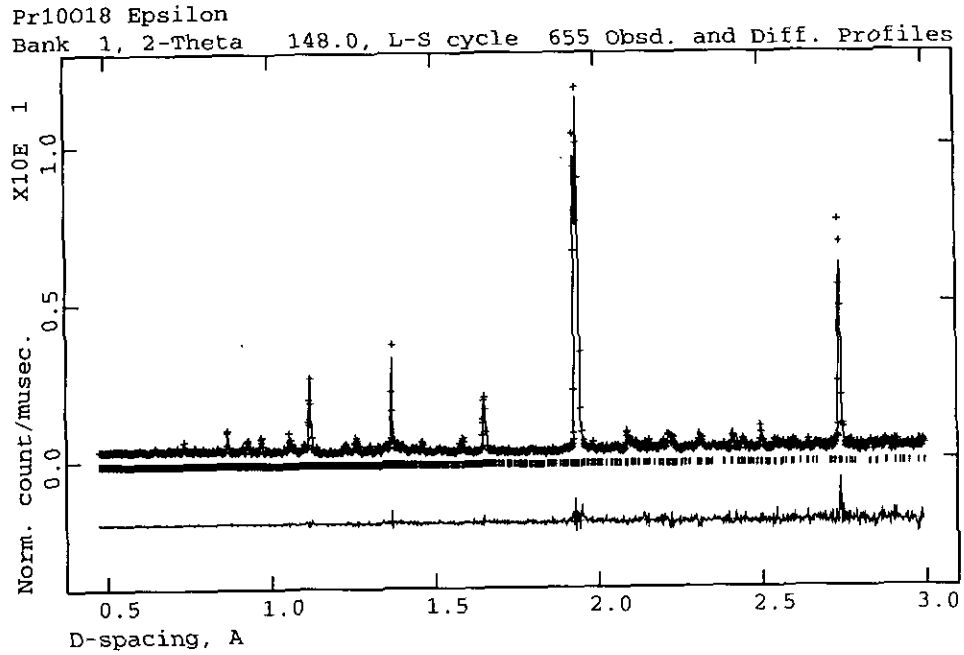

FIG. 2. The observed (crosses) and calculated (line) time-of-flight spectra for $Pr_{40}O_{72}$ (2θ at $+148°$) normalized by the incident intensity spectrum. The Bragg positions are marked.

TABLE 1
Important Refinement Parameters for $Pr_{10}O_{18}$

Diffractometer type	NPD		
No. of data in four spectra	26,545		
Minimum *d*-spacing (Å)	0.475		
Model	100% $Pr_{10}O_{18}$		
Space group	$P2_1/c$		
Lattice constants:			
a, *b*, *c* (Å)	6.7304(5)	19.390(1)	12.794(1)
β (°)	100.213(1)		
V (Å^3)	1643.2(4)		
Z	4		
Variables			
Structural:			
Lattice	4		
Positional	84		
Thermal	2		
Other			
Absorption	1		
Background	36		
Diffractometer	11		
Profile	8		
Scale	4		
Total	150		
wR_p (%)[a]	4.30		
R_p (%)[b]	2.93		
χ^2 (reduced)[c]	2.005		

[a] $wR_p = [w\Sigma(I_o-I_c)^2/\Sigma wI_o^2]^{1/2}$.
[b] $R_p = \Sigma|I_o-I_c|/\Sigma I_o$.
[c] $\chi^2 = \Sigma w(I_o-I_c)^2/(N_{obs}-N_{calc})$.

Careful examination of the difference curves suggested the presence of a second phase with a larger pseudo-fluorite cell, and the extra superstructure peaks corresponded to those of Pr_9O_{16}. Similar indications have been encountered during the structure refinements of other rare earth oxides, and it was found that introducing a second minor phase had very little effect on the structure determination of the major phase, although it might improve the refinement statistics. Therefore, the minor second phase was ignored since the refinement already involved numerous variables. The refined atomic parameters and important interatomic distances in $Pr_{10}O_{18}$ are reported in Tables 2 and 3, respectively. Figure 3 shows the $[1\ 0\ 0]_\varepsilon$ projection of the real structure of $Pr_{10}O_{18}$.

RESULTS AND DISCUSSION

The $[1\ 0\ 0]_\varepsilon$ projection of $Pr_{40}O_{72}$ determined from a Rietveld analysis of neutron TOF diffraction data is presented in Fig. 3. This solution corresponds to the model shown as Fig. 1c. The small yet significant distortions due to the formation of the vacancy clusters are also clearly portrayed in Fig. 3.

The relationship between the ε phase to the parent fluorite structures was determined by Kunzmann and Eyring (5) to be:

TABLE 2
Position and Thermal Parameters for $Pr_{10}O_{18}$

Atom	x	y	z	$U_{iso} \times 100$ (Å^2)[a] (Linked)
Pr(1)	0.3661(8)	−0.0070(3)	0.1175(5)	0.55(2)
Pr(2)	0.9025(9)	0.0983(4)	0.1192(5)	0.55(2)
Pr(3)	0.374(1)	0.1997(4)	0.1216(6)	0.55(2)
Pr(4)	0.8433(8)	0.3007(4)	0.1307(5)	0.55(2)
Pr(5)	0.382(1)	0.4112(3)	0.1288(5)	
Pr(6)	0.120(1)	0.0027(4)	0.3753(6)	0.55(2)
Pr(7)	0.6249(9)	0.0987(3)	0.3911(5)	0.55(2)
Pr(8)	0.1137(9)	0.1993(4)	0.3594(5)	0.55(2)
Pr(9)	0.6196(9)	0.2962(4)	0.3814(5)	0.55(2)
Pr(10)	0.123(1)	0.4004(4)	0.3670(5)	0.55(2)
O(1)	0.6593(8)	0.0140(3)	0.0726(3)	0.96(1)
O(2)	0.2365(7)	0.0958(3)	0.0742(4)	0.96(1)
O(3)	0.6791(8)	0.1937(3)	0.0828(4)	0.96(1)
O(4)	0.6772(8)	0.4033(3)	0.0774(4)	0.96(1)
O(5)	0.0644(9)	−0.0003(3)	0.1834(4)	0.96(1)
O(6)	0.0767(7)	0.2099(3)	0.1653(4)	0.96(1)
O(7)	0.5026(6)	0.3007(3)	0.1686(4)	0.96(1)
O(8)	0.0838(9)	0.3903(3)	0.1740(4)	0.96(1)
O(9)	0.4537(8)	0.0158(3)	0.2926(4)	0.96(1)
O(10)	0.8921(7)	0.1047(3)	0.2912(4)	0.96(1)
O(11)	0.4604(7)	0.1859(3)	0.3005(4)	0.96(1)
O(12)	0.9121(7)	0.2982(3)	0.3012(4)	0.96(1)
O(13)	0.4570(7)	0.3999(3)	0.3190(4)	0.96(1)
O(14)	0.8060(9)	0.0063(3)	0.4391(5)	0.96(1)
O(15)	0.3013(8)	0.1058(3)	0.4519(4)	0.96(1)
O(16)	0.8325(8)	0.1960(3)	0.4562(4)	0.96(1)
O(17)	0.2961(8)	0.2895(3)	0.4424(4)	0.96(1)
O(18)	0.8355(8)	0.3961(3)	0.4459(4)	0.96(1)
$V_o(1)$	3/16	3/10	1/16	—
$V_o(2)$	9/16	1/10	3/16	—

[a] The form of the isotropic displacement parameter is $T = \exp[-8\pi^2 U_{iso} \sin^2\theta/\lambda^2]$.

$$a'_\varepsilon = \tfrac{1}{2}(2a_F + b_F - c_F)$$
$$b'_\varepsilon = \tfrac{5}{2}(\quad + b_F + c_F)$$
$$c'_\varepsilon = 2(\quad - b_F + c_F).$$

The space group for this nonreduced cell is $P2_1/n$ (6, 7). By taking $c_\varepsilon = a'_\varepsilon + c'_\varepsilon$, the corresponding reduced cell should be (Fig. 1c)

$$a_\varepsilon = \tfrac{1}{2}(2a_F + b_F - c_F)$$
$$b_\varepsilon = \tfrac{5}{2}(\quad + b_F + c_F)$$
$$c_\varepsilon = \tfrac{1}{2}(2a_F - 3b_F + 3c_F)$$

also with $P2_1/c$ symmetry. The unit cell content is $Pr_{40}O_{72}$, four times $Pr_{10}O_{18}$, the formula for the $n = 10$ member.

There are 8 horizontal $(3\ \bar{3}\ 3)_F$ and 10 vertical $(0\ 2\ 2)_F$ oxygen planes in the ε unit cell (refer to Fig. 3). The location and number of vacant oxygen sites in the rows

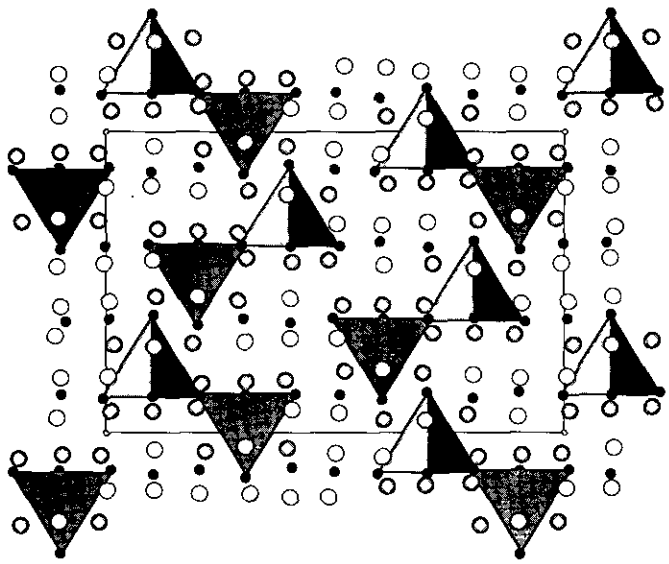

FIG. 3. The $[1\ 0\ 0]_\varepsilon$ projection of the ORTEP picture for $Pr_{40}O_{72}$. The oxygen (large circles) and the praseodymium (small circles) atoms are represented with 99% thermal ellipsoids. The Pr_4 tetrahedra around vacant oxygen sites are outlined.

and columns of the ε unit cells can be represented with sequences of (1111011110) for the $(0\ 2\ 2)_F$ and (11111111) for the $(3\ \bar{3}\ 3)_F$ oxygen planes of Fig. 1c. This, the observed structure, reflects the most uniform distribution of the vacancies. The previous model (7) (Fig. 1a) has the vacancies concentrated on selected $(3\ \bar{3}\ 3)_F$ planes with the pattern (22002200). There is a correlation here between the distribution of the vacant oxygen sites on the oxygen planes and the stability of a structure. The structure found experimentally has the most uniform vacancy distribution pattern.

The basic structural element in $Pr_{40}O_{72}$ is the double vacancy cluster, $[\square_O Pr_{(3+1/2)}O_6]_2$, as it was found to be in Pr_7O_{12}, Tb_7O_{12}, and Pr_9O_{16}. Two coordination defects $[\square_O Pr_4O_6]$ (16), sharing a common Pr are, in this structure, oriented along both the $[1\ 1\ 1]_F$ and the $[1\ \bar{1}\ \bar{1}]_F$ directions. The distortions from the fluorite structure follow patterns observed previously for the intermediate praseodymium and terbium oxides with $n < 10$. The 6-coordinated Pr remain approximately on their ideal fluorite positions, while the other Pr cations in the vicinity of vacant oxygen sites move away by about 0.2 Å. The six nearest oxygen atoms around each $\square_O$ move inward by about 0.3 Å. The $\square_O$–O distances within the coordination defects decrease with the vacancy concentration, i.e., it is 2.49 Å in Pr_7O_{12}, 2.437 Å in Pr_9O_{16}, and 2.406 Å in the most oxidized phase, $Pr_{24}O_{44}$. The two major causes of this may be that first, the lattice suffers a contraction as it becomes more oxidized (i.e., the formal fraction of Pr^{4+} increases); second, a lower vacancy concentration allows the oxygen anions

to be more tightly bound to the defect centers. Following the same general trend, the overall average $\square_O$–O distance is 2.419 Å in $Pr_{40}O_{72}$, falling between the values for Pr_9O_{16} and $Pr_{24}O_{44}$ as expected. (The chemical environments for the single vacancy defect clusters centered at $\square_O(1)$ and $\square_O(2)$ are not identical in $Pr_{40}O_{72}$; the corresponding $\square_O(1)$–O and $\square_O(2)$–O are 2.440 and 2.398 Å, respectively.) By analyzing the vacancy appearance pattern of the $(0\ 2\ 2)_F$ planes (0111101111), it is observed that the $\square_O(1)$'s are situated at the centers of the four consecutive $(0\ 2\ 2)_F$ planes containing vacancies, and as a result of the higher local vacancy concentration, the average $\square_O(1)$–O distance is relatively longer, whereas the $\square_O(2)$'s are near the $(0\ 2\ 2)_F$ planes that are defect free, consistent with a smaller average $\square_O(2)$–O distance.

The cations at the center of the cluster must become more oxidized with increasing n. For $n = 10$ we may have the formulation:

$$Pr^{4+} + (5Pr^{4+} + Pr^{3+}) + 3Pr^{3+}.$$

For $n = 11$ there would be no Pr^{3+} in the immediate environment of the oxygen vacancy.

By comparing the average Pr–O distances with the summation of the crystal radii (17), formal charges may be assigned to the Pr cations. The 6-coordinated Pr, Pr(3), is Pr^{4+}, and the three Pr's, Pr(6), Pr(9), Pr(10), in the defect-free region should be Pr^{3+}. The other six Pr's with coordination numbers of 7 bear formal charges between +3 and +4 (i.e., 3.83) as required by stoichiometry. These valence assignments require a charge separation in the structure. The defect clusters would be positively charged, while the defect-free regions would have net negative charges. As a consequence of the even distribution of the vacancies, the vacancy-free portion of the structure is divided into small pieces distributed among the clusters so that the strain introduced by the formation of defect clusters is reduced.

TABLE 3
Important Interatomic Distances in $Pr_{10}O_{18}$

Atom 1	Atom 2	Distance (Å)	Atom 1	Atom 2	Distance (Å)
		Pr coordination environment			
Pr(3)	O(2)	2.329(9)	Pr(1)	O(1)	2.418(9)
CN 6	O(3)	2.114(8)	CN 7	O(1)	2.284(9)
[+4][a]	O(6)	2.226(9)		O(2)	2.237(9)
	O(7)	2.113(8)		O(5)	2.29(1)
	O(11)	2.26(1)		O(9)	2.251(8)
	O(17)	2.28(1)		O(13)	2.268(9)
	Average	2.221		O(18)	2.34(1)
				Average	2.299
Pr(2)	O(1)	2.2371(9)	Pr(4)	O(3)	2.417(9)
CN 7	O(2)	2.421(8)	CN 7	O(4)	2.31(1)
	O(3)	2.355(9)		O(6)	2.361(9)
	O(5)	2.315(9)		O(7)	2.446(7)
	O(6)	2.426(9)		O(8)	2.38(1)
	O(10)	2.220(9)		O(12)	2.157(9)
	O(18)	2.179(9)		O(16)	2.215(9)
	Average	2.327		Average	2.326
Pr(5)	O(4)	2.220(8)	Pr(7)	O(4)	2.364(9)
CN 7	O(7)	2.273(8)	CN 7	O(9)	2.237(8)
	O(8)	2.209(9)		O(10)	2.390(8)
	O(9)	2.475(9)		O(11)	2.247(9)

TABLE 3—*Continued*

Atom 1	Atom 2	Distance (Å)	Atom 1	Atom 2	Distance (Å)
		O vacancy cluster			
$\square_{o(1)}$	Pr(3)	2.326(7)	Pr(3)	Pr(4)	4.111(9)
	Pr(4)	2.615(6)		Pr(5)	4.003(9)
	Pr(5)	2.568(6)		Pr(8)	4.003(9)
	Pr(8)	2.571(6)	Pr(4)	Pr(5)	4.197(9)
	Average[b]	2.585		Pr(8)	4.203(8)
			Pr(5)	Pr(8)	4.18(1)
$\square_{o(1)}$	O(6)	2.382(6)		Average[c]	4.116
	O(7)	2.301(5)			
	O(8)	2.446(6)			
	O(15)	2.487(5)			
	O(16)	2.531(5)			
	O(17)	2.493(5)			
	Average	2.440			
$\square_{o(2)}$	Pr(3)	2.429(7)	Pr(3)	Pr(1)	4.12(1)
	Pr(1)	2.570(6)		Pr(2)	4.044(8)
	Pr(2)	2.605(6)		Pr(7)	4.078(9)
	Pr(7)	2.560(6)	Pr(1)	Pr(2)	4.240(8)
	Average[b]	2.578		Pr(7)	4.183(8)
			Pr(2)	Pr(7)	4.228(8)
$\square_{o(2)}$	O(1)	2.443(6)		Average[c]	4.149
	O(2)	2.398(5)			
	O(3)	2.445(6)			
	O(9)	2.297(6)			
	O(10)	2.403(5)			
	O(11)	2.440(6)			
	Average	2.398			

Summation of crystal radii (Å)[d]

Pr^{m+}	CN = 6	CN = 7	CN = 8
$m = +3$	2.37	2.44	2.506
$m = +4$	2.23	2.29	2.34

[a] The charges are assigned by comparing the average distances with the corresponding summation of crystal radii (17).
[b] The average of the three $\square_O$–Pr where Pr CN = 7.
[c] The value is the average within the $\square_O Pr_4$ group.
[d] Values are from Ref. (17).

CONCLUSIONS

The unit cell of ε, $Pr_{40}O_{72}$, is monoclinic with $P2_1/c$ symmetry. The basic structural element is the double va-

cancy clusters in common with Pr_7O_{12}, Tb_7O_{12} and Pr_9O_{16}. In ε, however, these clusters are oriented along both the $[1\ 1\ 1]_F$ and $[1\ \bar{1}\ \bar{1}]_F$ directions. Their nature and arrangement follow common rules abstracted from the known structures of the other members of the R_nO_{2n-2} homologous series whose structures are known. It was found plausible to add another rule, i.e., that the most stable structure also exhibits the most uniform distribution of the vacant oxygen sites.

ACKNOWLEDGMENTS

It is a pleasure to acknowledge the patient tutorial help of D. J. M. Bevan in understanding the intricacies of these complex fluorite-related structures. We thank the National Science Foundation for financial support through Research Grant DMR-9114799 and the Manuel Lujan, Jr. Neutron Scattering Center, funded in part by the Office of Basic Energy Sciences Division of Materials Sciences of the U.S. Department of Energy (Contract W-7405-ENG-36).

REFERENCES

1. R. E. Ferguson, E. D. Guth, and L. Eyring, *J. Am. Chem. Soc.* **76,** 3890 (1954).
2. B. G. Hyde, D. J. M. Bevan, and L. Eyring, *Philos. Trans. R. Soc. London Ser A.* **259,** 583 (1966).
3. J. O. Sawyer, B. G. Hyde, and L. Eyring, *Bull. Soc. Chim. Fr.*, No. 149, 152 (1965).
4. R. P. Turcotte, M. S. Jenkins, and L. Eyring, *J. Solid State Chem.* **7,** 454 (1973).
5. P. Kunzmann and L. Eyring, *J. Solid State Chem.* **14,** 229 (1975).
6. R. T. Tuenge, R. B. Von Dreele, and L. Eyring, "Proceedings, 12th Rare Earth Research Conference, Vail, Colorado, July 18–20, 1976," p. 594, Denver Research Institute, Univ. of Denver.
7. R. T. Tuenge and L. Eyring, *J. Solid State Chem.* **29,** 165 (1979).
8. E. Schweda, L. Eyring, and D. J. Smith, *Ultramicroscopy* **23,** 443 (1987).
9. E. Schweda, D. J. M. Bevan, and L. Eyring, *J. Solid State Chem., p. 594,* **90,** 109 (1991).
10. A. C. Larson and R. B. Von Dreele, "GSAS—General Structure Analysis System," Los Alamos National Laboratory Report LA-UR 86-748 1986.
11. R. B. Von Dreele, L. Eyring, A. L. Bowman, and J. L. Yarnell, *Acta Crystallogr. Sect. B* **31**(4), 971 (1975).
12. J. Zhang, R. B. Von Dreele, and L. Eyring, *J. Solid State Chem.* in press.
13. J. Zhang, R. B. Von Dreele, and L. Eyring, *J. Solid State Chem.* **104,** 21 (1993).
14. J. Zhang, R. B. Von Dreele, and L. Eyring, submitted for publication.
15. J. Zhang, Z. C. Kang, and L. Eyring, *J. Alloys Compounds* **192,** 57 (1993).
16. R. L. Martin, *J. Chem. Soc. Dalton Trans.*, 1335, 1974.
17. R. D. Shannon, *Acta Crystallogr. Sect. A* **32,** 751, 1976.